INSTITUTE OF PHYSICS PUBLISHING PLASMA PHYSICS AND CONTROLLED FUSION

Plasma Phys. Control. Fusion **46** (2004) S81–S93 PII: S0741-3335(04)72022-9

Consistency of proposed burning plasma scenarios with alpha-particle transport induced by Alfvénic instabilities

G Vlad, S Briguglio, G Fogaccia and F Zonca

Associazione Euratom-ENEA sulla Fusione, CR Frascati, CP 65-I-00044-Frascati, Rome, Italy

E-mail: vlad@frascati.enea.it

Received 14 November 2003
Published 25 May 2004
Online at stacks.iop.org/PPCF/46/S81
DOI: 10.1088/0741-3335/46/7/S06

Abstract

The stability of proposed burning-plasma scenarios (for ITER-FEAT, IGNITOR and FIRE) with respect to shear-Alfvén modes possibly driven by fusion-produced alpha particles is investigated along with the effects of such modes on the transport and confinement properties of the alpha particles themselves. The results of numerical particle-in-cell model simulations show that one of the proposed scenarios (namely, the ITER-FEAT reversed-shear case) could be characterized by fast-growing energetic-particle modes, saturating via a convective displacement of the energetic ions. The consequent broadening pressure profile of the alpha particles and their additional diffusion due to scattering by the saturated electromagnetic fields show that the envisaged scenario cannot be considered consistent with the constraints imposed by nonlinear energetic-particle interactions with the Alfvén modes. The validity of the above results is discussed with reference to the approximations used in the model.

1. Introduction

In a burning plasma, fast ions (MeV energies) and charged fusion products (from now on referred to as fast or energetic ions) are expected to transfer their energy via Coulomb collisions to the thermal plasma particles (10 keV energies), providing thus a nuclear self-heating mechanism and a route to ignition. Due to their high velocity, they can resonate with and possibly destabilize Alfvén modes. Energetic-ion transport and confinement properties—of crucial importance for achieving efficient plasma heating and, therefore, ignition conditions—can in turn be affected by the nonlinear interaction with the Alfvénic modes themselves. Large efforts have then been devoted to assessing the stability of shear-Alfvén modes in tokamaks and, more recently, to their effect on the energetic-ion transport. Several instances providing evidence of rapid transient transport of energetic ions related with fluctuations in the frequency

range of Alfvén modes have been noted in plasmas heated with different auxiliary power systems, as discussed in [1, 2], and, as more recently reported, in the JT-60U tokamak [3] in connection with the so-called abrupt large amplitude events (ALEs). Meanwhile, particle-simulation studies have shown [4–6] that energetic-ion redistribution can take place because of fast-growing energetic-particle driven modes (EPMs) [7].

On the other hand, the operation scenarios for next-step proposed burning-plasma experiments (ITER-FEAT [8, 9], IGNITOR [10] and FIRE [11]) are usually obtained from equilibrium and transport codes that include a variety of thermal plasma transport models and, possibly, energetic ions and alpha-particle generation, slowing-down (SD), finite orbit width effects and ripple induced losses. However, none of the presently proposed scenarios consider the possibility that shear-Alfvén modes are excited and, eventually, produce macroscopic transport of the energetic particles themselves. Thus, a consistency problem of the envisaged burning-plasma scenarios can occur, in particular with reference to the alpha-particle radial profile and, therefore, to the fusion power radial distribution. In this respect, the issue of the dynamic behaviour of the system near marginal stability for collective mode excitation is certainly important [12]. Our goal, however, is not to consider the dynamics of scenario formation: taking a given scenario as reference, we rather address the simpler issue of describing nonlinear fusion product dynamics in such conditions and consider inconsistent those scenarios that are characterized by strongly unstable EPMs and macroscopic particle spatial redistributions [4–6]. The stability of the various equilibria with respect to the shear-Alfvén waves is investigated by means of the hybrid MHD–gyrokinetic code (HMGC) [4, 13, 14]. This simulation approach allows us to study the nonlinear evolution of unstable modes. Scenarios can be considered consistent with such nonlinear dynamics if energetic-particle pressure profiles in the presence of fully saturated modes are very close to the initial ones. On the contrary, strong differences between the two profiles (with and without shear-Alfvén mode dynamics) would prove the inconsistency of the corresponding scenario; these cases would then need more sophisticated tools to predict the equilibrium profiles.

Two scenarios are considered for ITER-FEAT [9, 15–17] as well as for IGNITOR [15, 18]: a monotonic-q (with q being the safety factor) and a reversed shear (RS) scenario. Only a monotonic-q case is instead examined for FIRE [15] since, at present, no RS scenario for this machine is available to the authors. Simulation results show that IGNITOR and FIRE scenarios are far from risks of inconsistency because the very low β_H value they present (with β_H being the ratio between alpha-particle and magnetic pressures) is well below the threshold for exciting EPM dynamics. Similar conclusions can be drawn for the monotonic-q ITER-FEAT scenario, though in this case the β_H threshold for the occurrence of alpha-particle redistribution is not exceedingly larger (within a factor of 2) than the nominal value. Finally, the RS ITER-FEAT scenario results in significant instability because of the fast-growing EPMs, which redistribute the alpha-particle source and flatten the corresponding β_H profile.

The structure of this paper is as follows. The numerical model used in the simulations is briefly discussed in section 2. Section 3 analyses the linear stability of the considered scenarios. Results about nonlinear EPM dynamics are presented in section 4, while section 5 is devoted to concluding remarks.

2. The model

The plasma model adopted in the particle-in-cell HMGC code consists [4, 13, 14] of a thermal plasma described by reduced $O(\epsilon^3)$ MHD equations [19, 20] (ϵ being the inverse aspect ratio of the torus), including resistivity and viscosity terms, and an energetic-particle population,

described by the nonlinear gyrokinetic equation [21, 22] simulated via particle-in-cell techniques. Energetic particles and thermal plasma are coupled through the divergence of the energetic-particle pressure tensor, which enters in the vorticity equation [23].

Numerical simulations are performed retaining, for each scenario, the relevant thermal-plasma parameters—the on-axis equilibrium magnetic field, safety factor, q, profile, the ion density, n_i—and the normalized alpha-particle pressure profile (β_H/β_{H0}, with β_{H0} being the on-axis β_H value). In most of the cases presented, the equilibrium magnetic configuration is instead approximated by assuming a large aspect ratio ($R_0/a = 10$). The quantity β_{H0} is then rescaled in order to preserve the desired value of the alpha-particle drive, $\alpha_H \equiv -R_0 q^2 \beta'_H$. Shifted circular magnetic surfaces are also assumed. The effect of Alfvén mode dynamics is examined by varying β_{H0} while keeping the profiles unchanged. We neglect, for simplicity, the nonlinear mode–mode coupling among different toroidal mode numbers, then limiting the analysis to the evolution of a single toroidal mode, n, while keeping fully nonlinear gyrokinetic dynamics for energetic particles. Fluid nonlinearities are indeed expected not to considerably alter EPM dynamics [4], whereas considering a single toroidal mode may underestimate the EPM effects on alpha-particle transport in the case of multi-n resonant overlap.

Note that neither the use of $O(\epsilon^3)$ MHD equations [19,20] nor the structure of the HMGC code itself poses actual limits on the aspect ratio values that can be studied, beyond those inherent in the model of Strauss *et al* [19]. The present assumption of $R_0/a = 10$ in most cases is due to the numerical convenience of allowing longer time steps, i.e. longer simulations at fixed resolution. In the following, we report on simulations made at the nominal aspect ratio values in order to justify the possibility of safely rescaling R_0/a while preserving the value of α_H.

The initial equilibrium distribution function of energetic particles in HMGC is assumed to be an isotropic Maxwellian, rather than a SD distribution function as in the case of fusion alpha particles; the characterizing parameters of the alpha-particle population are rescaled, however, in such a way as to reproduce wave–particle interactions, both with respect to the resonance frequency and the drive of the dominant Alfvén modes. In other words, we make the simulation Maxwellian (M) distribution function approximately equivalent to the SD physical one, as far as the wave–particle resonances are concerned. In order to do so, we have taken the analytic expression [24] for the energetic-particle kinetic contribution to the potential energy, δW_K, and computed it for both Maxwellian and SD distributions in the case of circulating particles. For fixed radial profiles, as assumed here, the only free parameters in the Maxwellian distribution are the energetic-particle thermal speed, $v_{H,M}$, and the density on the magnetic axis (or, equivalently, the parameter $\alpha_{H,M}$). 'Equivalence' of Maxwellian and SD distributions with respect to linear wave–particle interactions can then be obtained by prescribing these parameters in terms of the birth energy, $E_{\rm fus}$, and density of energetic particles (or $\alpha_{H,\rm SD}$) in the SD distribution, such that the 'distance' between the drive expressions ($\alpha_{H,M} v_{H,M} \delta W_{K,M}$ and $\alpha_{H,\rm SD} v_{H,\rm SD} \delta W_{K,\rm SD}$) is minimum. Here, $v_{H,\rm SD} \equiv (2E_{\rm fus}/m_H)^{1/2}$, with m_H being the energetic-particle mass. Approximately, this minimization procedure can be performed by matching the resonance frequency and the drive of the dominant Alfvén modes. From figure 1 it can be seen that the relationship needed to match the dominant energetic-particle resonance is $v_{H,M} \simeq 0.37 v_{H,\rm SD}$. For fusion alphas born at $E_{\rm fus} = 3.52\,$MeV, such a condition becomes $v_{H,M} \simeq 1.59 \times 10^{-2} c$. Similarly, matching the drive intensity then requires $\alpha_{H,M} v_{H,M} \simeq \alpha_{H,\rm SD} v_{H,\rm SD}/1.61$, that is $\alpha_{H,M} \simeq 1.68 \alpha_{H,\rm SD}$. Note that, for the present purposes, using a SD 'equivalent' Maxwellian is not a severe limitation. In fact, as stated in section 1, our goal is not to investigate the dynamics of scenario formation: we rather look at the possibility that strong particle redistributions are expected for a given scenario and at the inconsistency issue that this fact would pose. This physics is correctly accounted for, provided

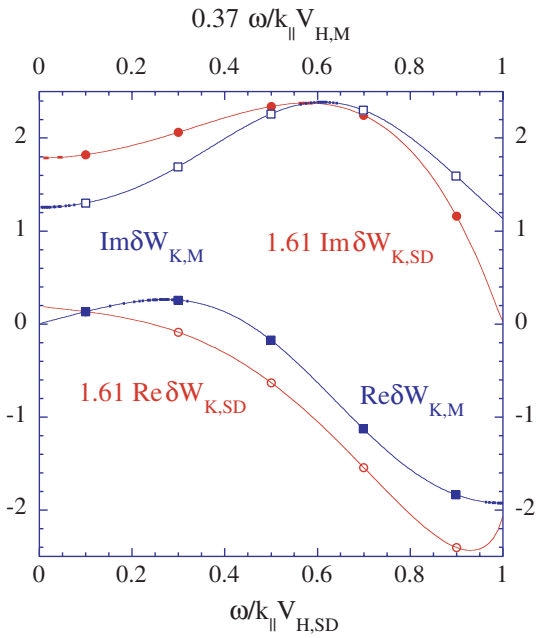

Figure 1. Energetic-particle kinetic contribution to the potential energy, δW_K, for Maxwellian (M, □, ■) and slowing-down (SD, ○, ●) distributions in the case of circulating particles. Matching the dominant resonance frequency requires $v_{H,M} \simeq 0.37 v_{H,\mathrm{SD}}$. It can be seen that, at maximum, $\mathrm{Im}\,\delta W_{K,M} \simeq 1.61 \mathrm{Im}\,\delta W_{K,\mathrm{SD}}$.

that linear wave–particle resonances are properly described—as it is by construction of the SD 'equivalent' Maxwellian—and the system is sufficiently away from marginal stability that 'weak' damping mechanisms such as electron [25] and ion [26] Landau damping can be neglected. For a sufficiently strong drive, mode and particle dynamics weakly depend on the velocity space detail of the distribution function. In contrast, the SD 'equivalent' Maxwellian assumption breaks down for marginal-stability studies [12], which are beyond the scope of this work. In the following, we will report the results in terms of the SD-equivalent parameters.

Simulation particles are loaded initially, for convenience, in the $(\mu, v_\parallel, \psi)$ space (μ, $v_\parallel$ being the magnetic moment and the parallel velocity of the energetic particles, and ψ the magnetic flux function, respectively): except for μ, these quantities are not canonical invariants of motion, and thus the initially loaded distribution function will relax, on a short timescale, to an equilibrium distribution function because of phase mixing. Typically, the relaxed distribution function is slightly broader in space than the original one.

3. Results: linear dynamics

Figure 2 shows the radial profiles of q, n_i (normalized to the on-axis value n_{i0}), β_H/β_{H0} and α_H (normalized to its maximum value $\alpha_{H\max}$) adopted in the simulations. For ITER-FEAT and IGNITOR, two different scenarios are considered: the respective monotonic-q-profile scenarios are reported in figures 2(a) [9] and (c) [15]; the corresponding RS cases are shown in figures 2(b) [16, 17] and (d) [18]. A monotonic-q-profile FIRE scenario [15] is shown

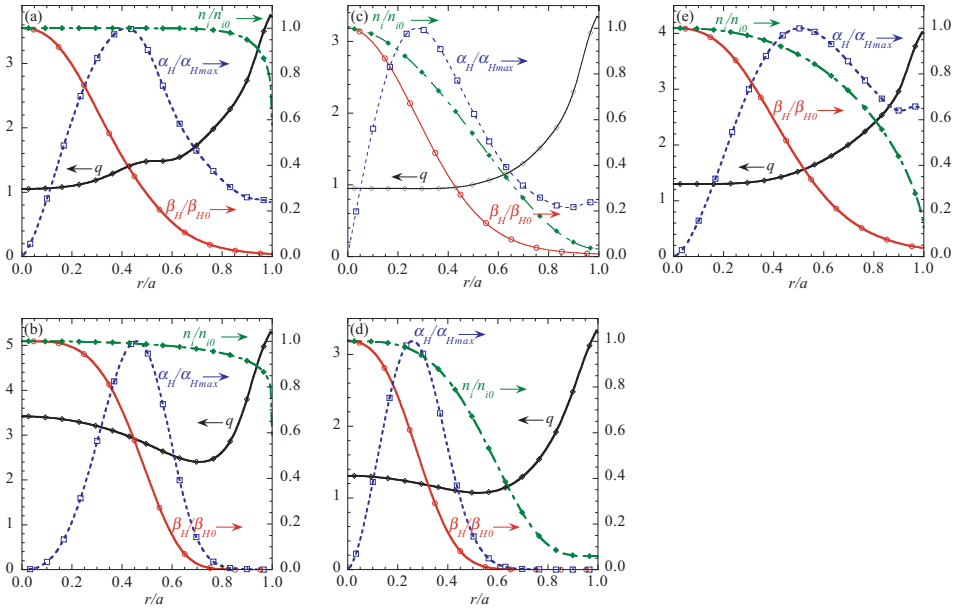

Figure 2. Radial profiles adopted in the simulations: q, n_i and β_H (normalized to their on-axis values, n_{i0} and β_{H0}, respectively), α_H (normalized to its maximum value, $\alpha_{H\max}$). Monotonic-q-profile equilibria are considered for ITER-FEAT (*a*), IGNITOR (*c*) and FIRE (*e*); RS profiles for ITER-FEAT (*b*) and IGNITOR (*d*).

Table 1. Relevant parameters for the scenarios represented in figure 2. The equivalent-Maxwellian simulation parameters are also reported. Here B is the toroidal magnetic field, T_{e0} and n_{e0} are the on-axis electron temperature and density (in the simulations, we have assumed $n_{i0} \approx n_{e0}$, v_{A0} is the on-axis Alfvén velocity, $P_{\rm fus}$ and $P_{\rm ext}$ are the fusion power and the external one, respectively).

	ITER-FEAT (*a*)	ITER-FEAT RS (*b*)	IGNITOR (*c*)	IGNITOR RS (*d*)	FIRE (*e*)
R_0 (m)	6.2	6.2	1.32	1.32	2.14
a (m)	2.0	1.86	0.48	0.48	0.6
B (T)	5.3	5.3	13.0	13.0	10.0
n_{e0} (10^{20} m^{-3})	1.02	0.73	9.4	12.36	4.9
T_{e0} (keV)	23.5	23.9	9.9	10.6	11.9
$\beta_{H0,\rm SD}$ %	0.91	0.95	0.16	0.24	0.23
$\beta_{H0,M}$ %	1.52	1.59	0.27	0.40	0.38
$\alpha_{H\,\max,\rm SD}$	0.098	0.78	0.0086	0.032	0.033
$\alpha_{H\,\max,M}$	0.53	3.90	0.053	0.19	0.15
$\rho_{H,\rm SD}/a$	0.0099	0.010	0.014	0.014	0.015
$\rho_{H,M}/a$	0.0094	0.010	0.016	0.016	0.017
$v_{H,\rm SD}/v_{A0}$	0.69	0.59	0.73	0.84	0.71
$v_{H,M}/v_{A0}$	0.66	0.56	0.82	0.93	0.77
$P_{\rm fus}$ (MW)	404.0	338.2	75.1	130.5	149.0
$P_{\rm ext}$ (MW)	34.1	67.7	30.0	11.2	12.5

in figure 2(*e*). Table 1 reports the relevant parameters for each scenario and those for the equivalent-Maxwellian simulations performed.

In figure 3 the growth rates of the dominant Alfvén modes are plotted versus $\beta_{H0}/\beta_{H0,\rm nom}$, for the considered scenarios, with $\beta_{H0,\rm nom}$ being the respective nominal on-axis β_H value.

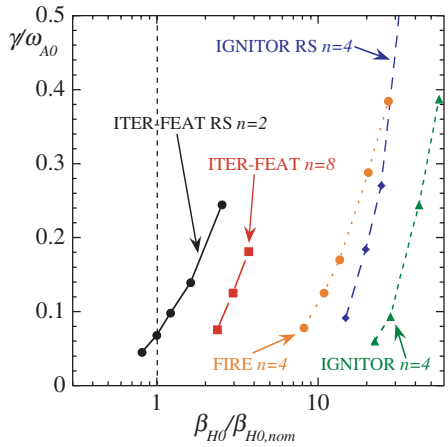

Figure 3. Growth rates of the most unstable modes (normalized to the on-axis Alfvén frequency) versus β_{H0} (normalized to the scenario nominal value, $\beta_{H0,\mathrm{nom}}$), for the scenarios considered in figure 2. The most unstable mode numbers come out to be $n = 2$ for the RS ITER-FEAT scenario; $n = 4$ for FIRE and both IGNITOR scenarios; $n = 8$ for the monotonic-q ITER-FEAT one. Fast-growing EPMs are unstable, for $\beta_{H0} = \beta_{H0,\mathrm{nom}}$, for ITER-FEAT RS.

Simulations for several toroidal mode numbers, n, have been performed ($n = 2, 4, 8, 12$) in order to identify the most unstable mode number, for each scenario. Our simulations show that the threshold for the destabilization of fast-growing energetic-particle modes (EPMs) [7] is very far from the operation regimes for both IGNITOR and FIRE. This is apparently due to the very low nominal β_{H0} value for such devices and, hence, to the very low alpha-particle drive in the Alfvénic modes. This is not the case for ITER-FEAT: the monotonic-q scenario is still stable, even though not very far from the instability threshold (less than a factor 2 in β_{H0}); the RS scenario is instead unstable, even at the nominal β_{H0} value. In the following we will then concentrate on the analysis of this device.

Precession resonance plays a dominant role in destabilizing EPMs, both in RS and monotonic-q ITER-FEAT scenarios. This can be seen by examining the following simulation results. Figure 4 shows the power spectra of scalar-potential fluctuations in the (r, ω) plane for different-n linearly unstable modes, both for the monotonic-q (top) and the RS (bottom) scenarios. The upper and lower Alfvén continuous spectra are also plotted, along with the precession frequency, $\omega_{d,H}(r) \simeq k_\theta \rho_H v_H / R_0$, the transit frequency, $\omega_{t,H}(r) \simeq v_H / R_0 q(r)$, and the maximum-$\alpha_H$ radial position, $r = \bar{r}$. Here $k_\theta \simeq nq(r)/r$ is the perpendicular wave vector, and ρ_H is the Larmor radius of the energetic particles. The results shown in this figure have been obtained in simulations characterized by β_{H0} values significantly larger than the EPM excitation threshold and refer to the linear-growth phase of the modes. We see that, for a given scenario and toroidal number, the modes tend to localize as close as possible to the intersection of the two curves $r = \bar{r}$ and $\omega = \omega_{d,H}$ ($\propto n$) while being quite insensitive to the localization of $\omega_{t,H}(r)$ (independent of n). In fact, the mode is not free to adapt exactly to the precession frequency because of the strong continuum damping it suffers as soon as its frequency departs from the gap in the Alfvén continuum [27, 28]. The most unstable toroidal number for each scenario is indeed that which causes $\omega_{d,H}(\bar{r})$ to fall within (or very close to) the gap: only for such modes does the need of maximizing the drive not conflict with the need for minimizing the damping; the other modes are compelled to find the best compromise between moderating the damping and exploiting the drive, and they waste a fraction of the potentially large resonant interaction.

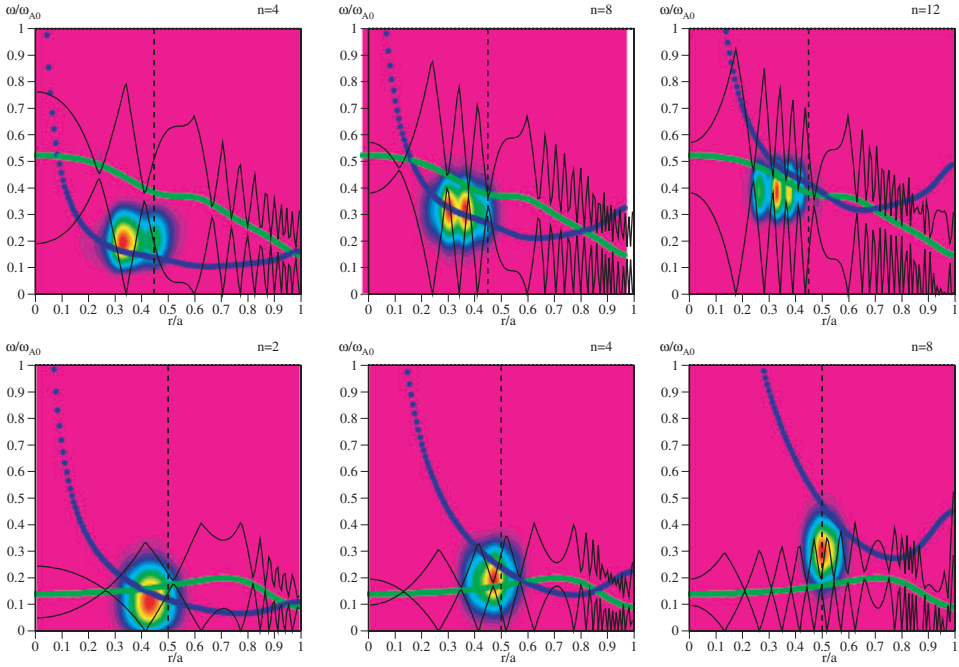

Figure 4. Power spectra of scalar-potential fluctuations in the $(r/a, \omega/\omega_{A0})$ plane for different-n linearly unstable modes, both for the monotonic-q (top) and the RS (bottom) ITER-FEAT scenarios. Upper and lower Alfvén continuous spectra are also plotted (black curves), along with the precession frequency (blue curve) and the transit frequency (green curve). The maximum-α_H radial position is indicated by the dashed line.

Note that because of the large values of q that characterize the RS scenario in the internal radial region (where the drive is maximum), the centre-of-the-gap frequency is much smaller in this than in the monotonic-q case. Such a feature implies that both the coincidence of $\omega_{d,H}(\bar{r})$ with the gap frequency and high-n orbit-averaging effects [24] (depressing the drive) take place for lower n in the former scenario than in the latter one. This explains why the most unstable situations occur for so different values of n in the two cases ($n = 2$ and 8, respectively).

Finally, the fact that the RS is more unstable than the monotonic-q scenario is due to the very different amounts of energetic-particle drive for the two cases: in spite of very similar values of the nominal β_{H0}, the RS case is characterized by a much larger value of $\alpha_{H\max}$ than the monotonic-q one because of the larger value of q and the steeper β_H radial profile (cf table 1).

Before testing the consistency of the RS ITER-FEAT scenario against the nonlinear evolution of these unstable modes, it is worth checking the reliability of the main approximation adopted in these simulations: namely, the large aspect-ratio (R_0/a). In figure 5 (left), the effect of reducing the aspect ratio on the Alfvén continua is shown: the toroidal gap clearly widens for smaller R_0/a, and a mode excited within the frequency gap will typically suffer less continuum damping [27, 28]. The growth rates for the approximated ($R_0/a = 10$) RS ITER-FEAT scenario (with correspondingly rescaled β_{H0}) are compared, in figure 5 (right), with those obtained for the actual value, $R_0/a \simeq 3.3$. Modes with $n = 4$ are considered in this case. Slightly higher growth rates are in fact observed for smaller R_0/a, consistent with the changes in the continuous spectrum.

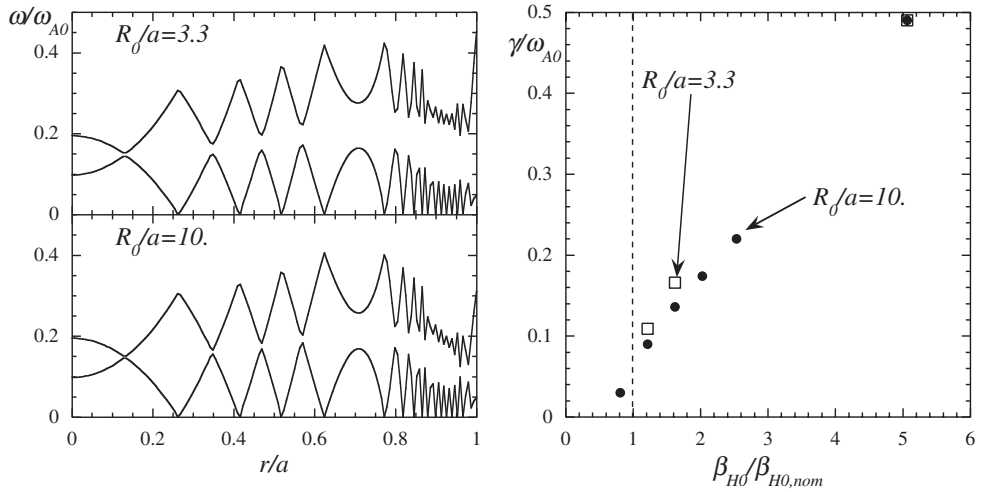

Figure 5. Left: toroidal Alfvén continuous spectra, in the RS ITER-FEAT case, for $R_0/a \simeq 3.3$ (the nominal value) and $R_0/a = 10$ (the value used in the large-aspect-ratio simulations). Right: $n = 4$ EPM growth rates versus $\beta_{H0}/\beta_{H0,\mathrm{nom}}$, for the two different values of R_0/a.

A more subtle remark is needed for the expected difference in the dominant mode numbers due to rescaling of R_0/a. Most unstable modes are characterized by $k_\theta \rho_B \approx 1$, where now ρ_B is the banana/drift orbit width for trapped/circulating particles. No effect of R_0/a rescaling on the most unstable mode numbers is expected in the case of dominant transit resonance ($k_\theta \rho_B \simeq nq^2\rho_H/r$). For dominant precession resonance ($k_\theta \rho_B \simeq nq^2(R_0/r)^{1/2}\rho_H/r$), on the contrary, considering higher R_0/a values would result in lower dominant toroidal mode numbers and in underestimating the growth rates of the large-n portion of the spectrum. Because of the q^{-2} dependence of the most unstable n, this effect is expected to be more relevant for the monotonic-q case ($q(\bar{r}) \simeq 1$) than for the RS one ($q(\bar{r}) \simeq 3$). Our analysis can then be considered quite optimistic in determining the stability properties of each scenario (especially the former one).

4. Results: nonlinear dynamics

The phenomenology of nonlinear wave–particle dynamics for the ITER-FEAT RS scenario (with $\beta_{H0} = \beta_{H0,\mathrm{nom}}$) is shown in figure 6. The simulation shows that, after the *linear-growth* phase, the mode saturates because of a relevant radial displacement of the energetic-particle source. Such a convective displacement is analogous to that described in [5,6], where it has been indicated as an *avalanche* phase. Significant diffusion of energetic particles continues during the entire following *saturated* field-amplitude phase because of energetic-particle scattering in the saturated electromagnetic fields. This evolution is represented in figure 6, where the power spectra of scalar-potential fluctuations are reported for three times (top frames): during the linear growth of the mode (left) at the end of the avalanche phase (centre) and in the saturated regime (right). The corresponding β_H profiles and the radial profiles of the Fourier components of the fluctuating scalar potential are plotted in the middle and bottom frames of the same figure, respectively.

The distinction between the linear, avalanche and saturated phases is further illustrated in figure 7, which shows the time dependence of the radial position at which the maximum

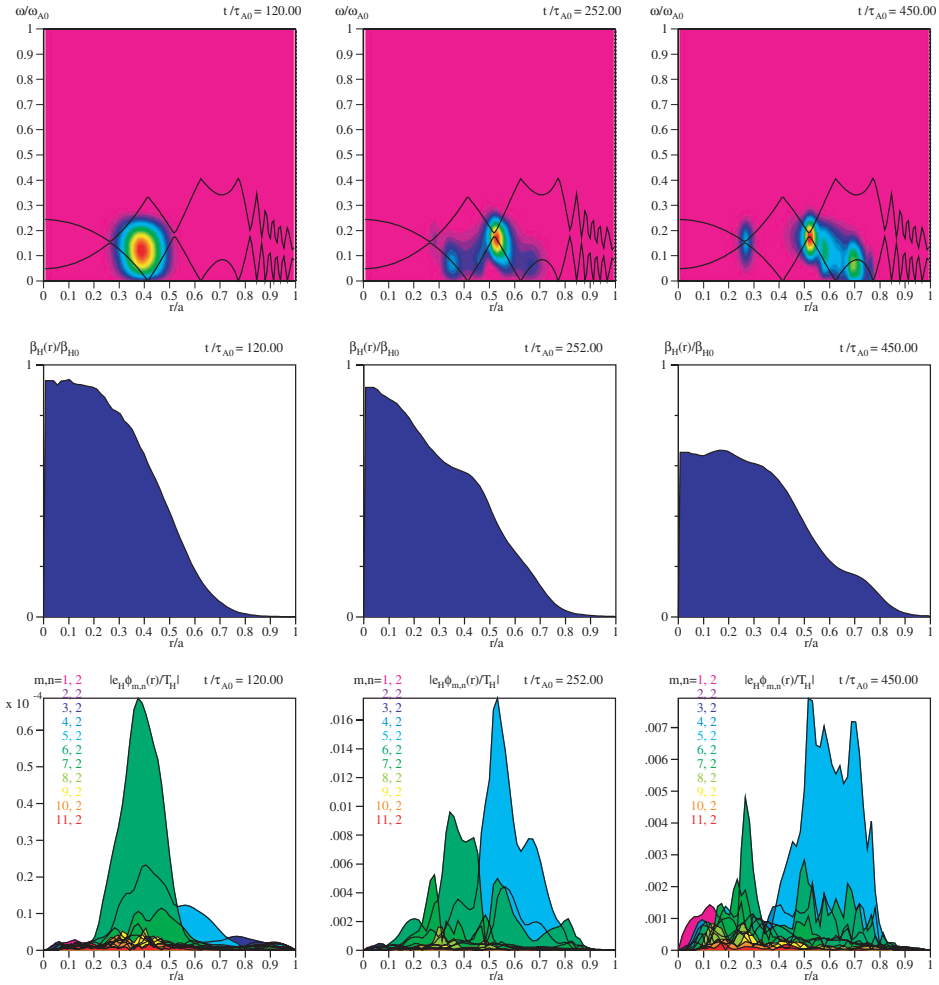

Figure 6. Power spectra of scalar-potential fluctuations in the $(r/a, \omega/\omega_{A0})$ plane with the shear Alfvén continuous spectrum superimposed (top), β_H profiles (middle) and radial profiles of the m, n Fourier components of the fluctuating scalar potential (in units of T_H/e_H, with e_H being the electric charge of the energetic particles, bottom) for the RS ITER-FEAT scenario ($\beta_{H0} = \beta_{H0,\mathrm{nom}}$), at three different stages: linear growth (left), end of the avalanche phase (centre), saturated phase (right). The slight departure, in the linear-growth phase, of the on-axis β_H from its initial value, β_{H0}, is due to the relaxation process discussed at the end of section 2.

of the radial gradient of the energetic-particle profile occurs along with the magnitude of the maximum gradient itself. The steepening of the gradient and the rapid outward shift of the maximum-gradient radial position characterize the avalanche (convective) phase as an unstable propagating front. The following, slower, decay of the maximum-gradient magnitude corresponds to the saturated (diffusive) phase.

To quantify the convection generated by the nonlinear EPM evolution, we introduce the quantity $(r/a)_y$, defined as the radial surface enclosing the fraction y of the energetic-particle energy content and given implicitly by

$$y = \frac{\int_0^{(r/a)_y} x\beta_H(t,x)\,\mathrm{d}x}{\int_0^1 x\beta_{H,\mathrm{init}}(x)\,\mathrm{d}x} \tag{1}$$

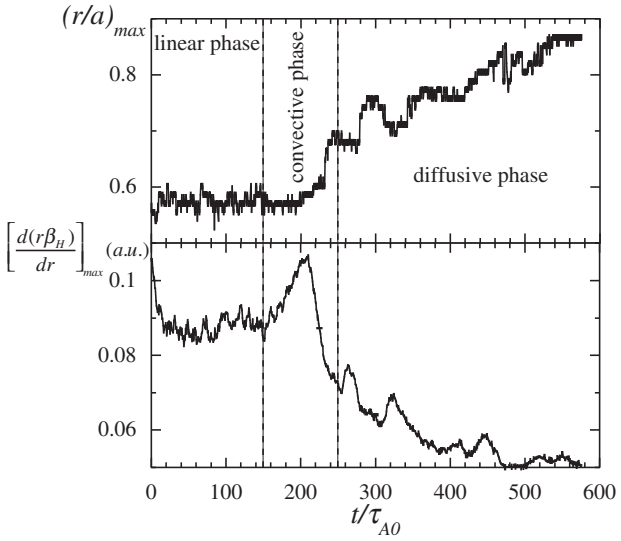

Figure 7. Radial position (top) and value (bottom) of the maximum gradient of $r\beta_H$ versus time, for the same case presented in figure 6. The strong convection, characteristic of the *avalanche phase*, and the diffusion, which takes place in the *saturated phase*, can be recognized.

with $\beta_H(t, x)$ being the energetic-particle pressure profile and $\beta_{H,\mathrm{init}}(x)$ being the 'initial' (i.e. relaxed, in the sense discussed in section 2) profile. An increase in $(r/a)_y$ with t then corresponds to a radial broadening of the energetic-particle source.

The diffusion characterizing the saturated phase can be quantified by defining the typical diffusive time, $\tau_{\mathrm{diff},y}$, as

$$\tau_{\mathrm{diff},y} \equiv \left(\frac{r}{a}\right)_y \left[\frac{\mathrm{d}}{\mathrm{d}t}\left(\frac{r}{a}\right)_y\right]^{-1}. \tag{2}$$

The results concerning nonlinear saturation are shown, for all the devices/scenarios considered, in figure 8 (left), where $(r/a)_{85\%}$ at the end of the avalanche phase is plotted versus $\beta_{H0}/\beta_{H0,\mathrm{nom}}$. For each scenario, the horizontal segment corresponds to the EPM-free regime. In figure 8 (right) the values of the inverse diffusion time, $\tau^{-1}_{\mathrm{diff},85\%}$, characterizing the saturated phase are shown for the same cases. These results quantify the possible inconsistency of the ITER-FEAT RS scenario with respect to the EPM dynamics: at the nominal value, $\beta_{H0}/\beta_{H0,\mathrm{nom}} = 1$, the radial surface enclosing 85% of the energetic-particle energy is observed to be displaced, at the end of the convective phase, by more than 10%. Moreover, a significant transport still persists during the saturated phase, corresponding to a diffusive time $\tau_{\mathrm{diff},85\%} \simeq 1.6 \times 10^3 \tau_{A0}$. Both effects increase rapidly with β_{H0}.

5. Conclusions

The issue of the stability of burning-plasma scenarios with respect to shear-Alfvén modes driven by fusion-generated alpha particles has been addressed by means of particle-in-cell numerical simulations. The effects of the nonlinear dynamics of such modes on the transport and confinement properties of the alpha particles themselves have been investigated, and the consistency of the proposed scenarios—normally determined on the basis of transport codes that neglect possible collective alpha-particle effects—has been discussed.

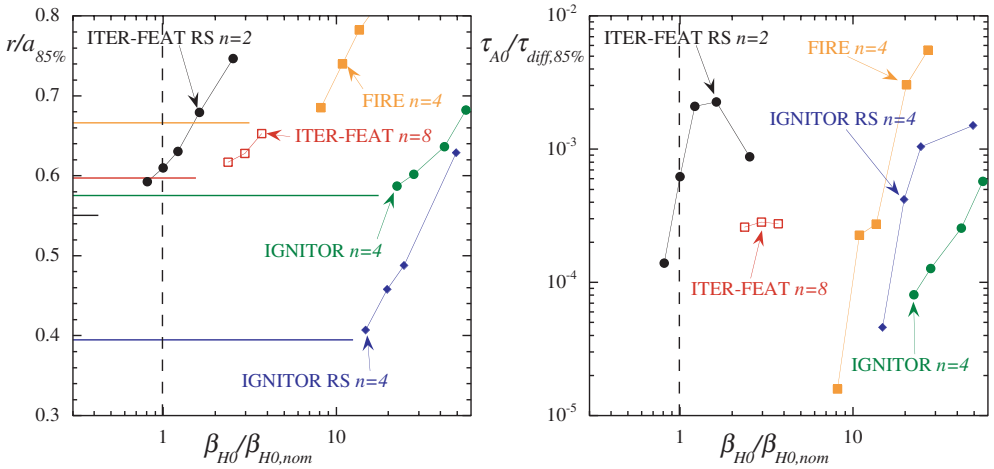

Figure 8. Left: radial positions of the surface containing 85% of the alpha-particle energy versus $\beta_{H0}/\beta_{H0,\mathrm{nom}}$, for the scenarios considered in figure 2. The most unstable toroidal number is considered for each scenario. The horizontal segments represent, for each scenario, the EPM-free regime. Right: the inverse of the diffusion time, $\tau_{\mathrm{diff},85\%}$ (normalized to the on-axis Alfvén time), versus $\beta_{H0}/\beta_{H0,\mathrm{nom}}$, for the same cases.

The examined scenarios for IGNITOR and FIRE are found to be free from resonant collective alpha-particle effects because of the very low values of the alpha-particle pressure (compared with the magnetic pressure) that characterize the respective operation regimes. The same conclusion is reached for ITER-FEAT, as far as the monotonic-q scenario is considered, though the device would operate, in this case, more closely to the threshold for the excitation of resonant modes. The RS scenario, characterized by much larger amount of alpha-particle resonant drive (both because of the steeper β_H gradient and the higher value of q in the maximum-gradient region), is instead unstable with respect to predicted fast-growing EPMs. These modes saturate via convective radial outward displacement of alpha particles and consequent broadening of the relative β_H profile. Also, additional broadening takes place because of a slower diffusion of energetic particles scattered by the saturated electromagnetic fields. These results indicate that constraints posed by the nonlinear interaction between energetic particles and shear-Alfvén modes should be taken into account for the RS ITER-FEAT scenario to obtain reference fusion-product profiles consistent with the shear-Alfvén mode dynamics.

Some caution has to be exercised in drawing conclusions from the present results because of the approximation adopted in the numerical model. The most delicate aspect is represented by the large aspect ratio assumption. Such an approximation, adopted here for numerical convenience, is consistent with the small-ϵ expansion, which provides a basis for the reduced-MHD model [19].

We have shown that, for the toroidal mode numbers examined in the paper, a satisfactory agreement is found between the realistic-ϵ results and the small-ϵ approximation, provided that the on-axis β_H value is rescaled, in the latter case, to preserve the drive intensity, α_H. The present results also show that the growth rates found for the nominal ϵ value of the ITER-FEAT RS scenario are slightly larger than the approximated ones.

Thus, our conclusions on the potential inconsistency of burning plasma scenarios are adequately independent of the small-ϵ approximation.

It cannot however be ruled out that a thorough analysis of the realistic-ϵ case would show that, especially for low-q scenarios, larger ns are most unstable and/or other resonances (transit or bounce) are more relevant than the precession resonance, which dominates wave–particle interactions in the present analyses. In any case, this would correspond to an even more unstable situation.

Finally, further effects on energetic-ion transport could be found in the framework of a more complete analysis including multiple-n dynamics. In order to reproduce correctly the effect of resonance-overlap in particle phase space, such an analysis should be performed at the nominal ϵ value.

Generally speaking, we can conclude that the R_0/a rescaling, adopted here for numerical convenience, provides an optimistic picture of the possible detrimental effects on energetic-ion transport due to resonant EPM excitations. Our warning on scenario-consistency problems in burning plasmas is therefore valid *a fortiori*.

Although an isotropic Maxwellian rather than a SD distribution function of energetic particles has been used in HMGC, particular care has been devoted to reproducing best the wave–particle interactions, both with respect to the resonance frequency and the drive of the dominant Alfvén modes during the linear phase. This approximation is not expected to affect significantly nonlinear particle behaviours sufficiently away from marginal stability, as already discussed in section 2.

Several damping mechanisms are neglected in our model. Among them, the most relevant should be thermal ion Landau damping, γ_{iLD}, and trapped electron collisional damping, γ_e. A simple estimate [29], evaluated for the ITER-FEAT RS case with toroidal mode number $n = 2$ (the most critical scenario considered), gives $\gamma_{\mathrm{iLD}}/\omega \simeq 0.11$ and $\gamma_e/\omega \simeq 0.0085$ at the radial position where the mode has linear growth rate $\gamma/\omega_{A0} \simeq 0.068$ and real frequency $\omega/\omega_{A0} \simeq 0.12$. Thus, both the neglected dampings are small compared with the calculated growth rate ($\gamma_{\mathrm{iLD}} \simeq 0.2\gamma$ and $\gamma_e \simeq 0.015\gamma$).

In spite of the limitations discussed, the study presented here is the first attempt to make predictions on the relevance of nonlinear Alfvén mode dynamics in burning plasmas.

References

[1] Heidbrink W W and Sadler G J 1994 *Nucl. Fusion* **34** 535
[2] Wong K L 1999 *Plasma Phys. Control. Fusion* **41** R1
[3] Shinohara K *et al* 2001 *Nucl. Fusion* **41** 603
[4] Briguglio S, Zonca F and Vlad G 1998 *Phys. Plasmas* **5** 3287
[5] Briguglio S, Vlad G, Zonca F and Fogaccia G 2002 *Phys. Lett.* A **302** 308
[6] Vlad G, Briguglio S, Fogaccia G and Zonca F 2002 *Proc. 29th EPS Conf. (Montreux, 2002)* vol 26B (ECA) P-4.088
[7] Chen L 1994 *Phys. Plasmas* **1** 1519
[8] ITER Physics Basis Editors *et al* 1999 *Nucl. Fusion* **39** 2137
[9] Aymar R *et al* 2000 *Proc. 18th Int. Fusion Energy Conf. (Sorrento, 2000)* (Vienna: IAEA) paper IAEA-CN-77/ITEROV/1
[10] Coppi B, Airoldi A, Bombarda F, Cenacchi G, Detragiache P, Ferro C, Maggiora R, Sugiyama L E and Vecchi G 1999 Critical physics issues for ignition experiments: Ignitor *Report* MIT RLE PTP 99/06
[11] Meade D 2000 *Comments Plasma. Phys. Control. Fusion* **2** 81
[12] Berk H L, Breizman B N and Pekker M S 1997 *Plasma Phys. Rep.* **23** 778
[13] Vlad G, Kar C, Zonca F and Romanelli F 1995 *Phys. Plasmas* **2** 418
[14] Briguglio S, Vlad G, Zonca F and Kar C 1995 *Phys. Plasmas* **2** 3711
[15] Budny R V 2002 *Nucl. Fusion* **42** 1383
[16] Polevoi A R, Medvedev S Yu, Mukhovatov V S, Kukushkin A S, Murakami Y, Shimada M and Ivanov A A 2002 *J. Plasma Fusion Res. Ser.* **5** 82
[17] Gormezano C and Gribov Y 2003 private communication

[18] Cenacchi G and Romanelli M 2003 private communication
[19] Strauss H R 1977 *Phys. Fluids* **20** 1354
[20] Izzo R, Monticello D A, Park W, Manickam J, Strauss H R, Grimm R and McGuire K 1983 *Phys. Fluids* **26** 2240
[21] Frieman E A and Chen L 1982 *Phys. Fluids* **25** 502
[22] Lee W W 1987 *J. Comp. Phys.* **72** 243
[23] Park W *et al* 1992 *Phys. Fluids* B **4** 2033
[24] Zonca F and Chen L 1996 *Phys. Plasmas* **3** 323
[25] Chen L 1989 *Theory of Fusion Plasmas (Varenna, 1988)* ed J Vaclavik *et al* (Bologna: Editrice Compositori) p 327
[26] Betti R and Freidberg J P 1992 *Phys. Fluids* B **4** 1465
[27] Zonca F and Chen L 1992 *Phys. Rev. Lett.* **68** 592
[28] Zonca F and Chen L 1993 *Phys. Fluids* B **5** 3668
[29] Romanelli F and Zonca F 1994 *Tokamak Concept Improvement (Varenna, 1994)* ed S Bernabei *et al* (Bologna: Editrice Compositori) p 191